A Case Study of an Outbreak of Twin Tropical Cyclones

CARL J. SCHRECK III AND JOHN MOLINARI

Department of Earth and Atmospheric Sciences, University at Albany, State University of New York, Albany, New York

(Manuscript received 24 January 2008, in final form 13 June 2008)

ABSTRACT

Previous studies have found that twin tropical cyclogenesis typically occurs 2–3 times a year in the Pacific Ocean. During October 1997, however, three sets of twin tropical cyclones developed in the central Pacific within a single month. Tropical cyclone archives indicate that this is the only such outbreak from 1969 to 2006. This case study explores the background and synoptic conditions that led to this unique event. All three twin tropical cyclogenesis events occurred within a broad and long-lasting envelope of warm water, low surface pressure, active convection, and weak or easterly vertical shear. Westerly winds at the equator and trade easterlies farther poleward created strips of cyclonic vorticity through a deep layer. A low-pass filter showed that these favorable conditions shifted eastward with time at 1–2 m s^{-1}. In addition to the gradual eastward movement, the equatorial westerlies and convection were modulated by higher-frequency westward propagation. These anomalies appear to have been associated with convectively coupled $n = 1$ equatorial Rossby waves. The twin tropical cyclones formed only when the sum of the two modes produced equatorial westerlies in excess of 5 m s^{-1} and brightness temperature below 270 K. Applications of these results are proposed for the operational prediction of twin tropical cyclogenesis.

1. Introduction

Tropical cyclones occasionally form on opposite sides of the equator at nearly the same time and longitude. A climatology by Keen (1982) found that these twin tropical cyclones developed 2.4 times a year in the Pacific Ocean. Lander (1990) used a stricter definition to determine that twin tropical cyclones of typhoon intensity formed once every two or three years globally. In the central Pacific, Harrison and Giese (1991) observed that twin tropical cyclones happened once every five years. By any of these definitions, twin tropical cyclogenesis is a relatively uncommon event. However, three sets of twin tropical cyclones, producing seven storms, developed in the central Pacific during the month of October 1997. The present case study addresses the conditions that led to this outbreak.

Lander (1990) showed that twin tropical cyclones are often preceded by deep convection along the equator associated with near-gale-force equatorial westerlies. He argued that these westerlies were part of the equatorial Rossby (ER) wave response to convective heating described by Gill (1980). Lander suggested that the twin tropical cyclones ultimately form within the equatorially symmetric cyclonic vorticity associated with this convectively forced ER wave.

An idealized study by Ferreira et al. (1996) proposed a similar mechanism for twin tropical cyclogenesis. The Gill (1980) solution describes the tropical response to stationary heating (mass sink) in a linear shallow water model, but Ferreira et al. tested this response in a nonlinear model. In these nonlinear experiments, twin cyclonic vortices developed within the forced ER wave. These vortices could act as seedlings for twin tropical cyclones. The heating in their model represented the diabatic heating associated with any super cloud cluster, but they noted that it could correspond to the Madden–Julian oscillation (MJO; Madden and Julian 1971) in particular.

To expand the analogy to the MJO, Ferreira et al. (1996) performed an additional experiment with a more complicated heat source. The heating was initially held stationary, then gradually moved eastward with constant strength, and finally became stationary again as it dissipated. They argued that this mimicked the observed

Corresponding author address: Carl J. Schreck III, Dept. of Earth and Atmospheric Sciences, University at Albany/SUNY, ES-330, Albany, NY 12222.
E-mail: carl@atmos.albany.edu

DOI: 10.1175/2008MWR2541.1

life cycle of the MJO as it develops in the Indian Ocean, moves eastward across Indonesia, and then decays near the date line. In this simulation, the heating produced trailing strips of cyclonic vorticity as it moved eastward. However, the cyclonic vortices developed only in the regions where the heating remained stationary; that is, where the simulated MJO developed and decayed.

Liebmann et al. (1994) argued that any slowly varying convective system, like the MJO, could enhance climatologically favorable conditions to produce clustering of tropical cyclones. They found that the MJO creates a region of low-level cyclonic vorticity and convergence that should favor cyclogenesis. Although Liebmann et al. did not specifically address twin tropical cyclones, their results showed favorable regions for tropical cyclogenesis concurrently in both hemispheres (e.g., their Fig. 5).

The low-level cyclonic vorticity associated with the MJO could represent an ER wave that is forced by the convection (Ferreira et al. 1996). However, a number of recent studies have also investigated equatorial waves that are coupled with convection (e.g., Takayabu 1994; Wheeler and Kiladis 1999; Yang et al. 2003; Roundy and Frank 2004). Convectively coupled equatorial waves typically propagate like the shallow water solutions derived by Matsuno (1966) for equivalent depths of 12–50 m (Wheeler and Kiladis 1999). These coupled waves feature enhanced convection in the regions where the linear solutions exhibit low-level convergence.

Several studies have investigated the impacts of convectively coupled equatorial waves on tropical cyclogenesis (e.g., Numaguti 1995; Dickinson and Molinari 2002; Bessafi and Wheeler 2006; Frank and Roundy 2006; Molinari et al. 2007). These studies found that convectively coupled waves influence cyclogenesis primarily by modulating convection and low-level vorticity. While none of these studies discussed twin tropical cyclones explicitly, some of the convectively coupled waves exhibit structures that are equatorially symmetric, such as $n = 1$ ER waves. These symmetric waves could simultaneously enhance conditions for cyclogenesis in both hemispheres and lead to twin tropical cyclones.

Keen (1982) found that El Niño conditions can favor twin tropical cyclones in the central Pacific. The anomalous circulation during El Niño features broader equatorial westerlies and near-equatorial troughs within which the twin tropical cyclones may form. Keen also suggested that the tropical cyclones could in turn strengthen the equatorial westerlies channeling between them. This feedback might enhance the El Niño by expanding the warm water eastward. However, Lander (1990) observed that the equatorial westerlies actually weaken as the twin tropical cyclones form and intensify. Harrison and Giese (1991) found no clear relationship between twin tropical cyclones and equatorial westerlies, with the westerlies sometimes peaking before and sometimes after cyclogenesis.

Figure 1 shows a time series of the Niño-3.4 index anomalies (black curves) and twin tropical cyclogenesis (vertical lines). The Niño-3.4 index is obtained from the Climate Prediction Center and has been smoothed with a 5-month running mean. The vertical lines in Fig. 1 indicate months in which twin tropical cyclogenesis occurred in the Joint Typhoon Warning Center's (JTWC) best-track dataset using the definitions proposed by Keen (1982; Fig. 1a) and Harrison and Giese (1991; Fig. 1b). Lander's (1990) definition lacks quantitative criteria for such a plot. Cyan lines show months in which one set of twin tropical cyclones formed, blue lines indicate two events, and red lines show three events. October 1997 is the only month from 1969 to 2006 in which either definition found three events.

Regardless of the definition for twin tropical cyclogenesis, such events happen more frequently during El Niño conditions (Fig. 1). The median Niño-3.4 anomaly for twin tropical cyclogenesis events is 0.34°C using Keen's (1982) definition and 1.06°C using Harrison and Giese's (1991) definition. Harrison and Giese only examined central Pacific storms, which explains the stronger signal with that definition (Fig. 1b). The Niño-3.4 anomalies are also greater than zero during every month in which multiple twin tropical cyclogenesis events occurred (blue and red lines). Figure 1 illustrates that the three twin tropical cyclogenesis events of October 1997 (red line) formed near the peak of the strong 1997–98 El Niño. In contrast, no twin tropical cyclones formed during the similarly intense 1982–83 El Niño event, which suggests that El Niño by itself is not a sufficient condition for twin tropical cyclone outbreaks.

The present study will investigate the conditions that led to the three twin tropical cyclogenesis events in the central Pacific during October 1997. Figure 2 shows a time–longitude plot of all tropical cyclogenesis events that occurred equatorward of 15° latitude in the Pacific Ocean from 10 September to 19 November. The red-filled hurricane symbols indicate Northern Hemisphere storms, while blue-filled symbols denote Southern Hemisphere storms. The green circles highlight the twin tropical cyclones.

Figure 2 presents a relatively active period for cyclogenesis in the Pacific with 20 storms developing over 70 days. Consistent with the intense El Niño event of 1997–98 (Fig. 1), many of these tropical cyclones form in the central Pacific (Lander and Guard 2001). Four storms even develop in the South Pacific, which is

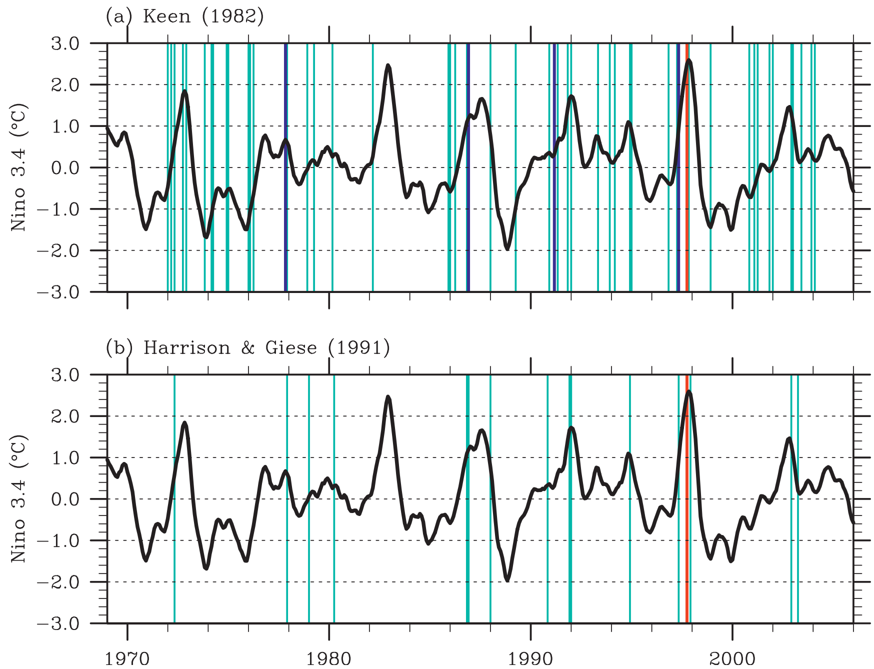

FIG. 1. Time series plots of Niño-3.4 index anomalies smoothed with a 5-month running mean. Vertical lines indicate months in which one (cyan), two (blue), or three (red) twin tropical cyclogenesis events occurred using the definitions of (a) Keen (1982) and (b) Harrison and Giese (1991).

usually inactive during this time of year (Frank and Roundy 2006). Of these four Southern Hemisphere tropical cyclones, three are associated with twin tropical cyclogenesis events.

The first event begins with the formation of a South Pacific storm on 4 October. This set of "twins" is somewhat unconventional as it includes two Northern Hemisphere storms that develop over the next 6.75 days. These three storms form west of the date line and within 9° longitude of each other. The remaining two sets of twin tropical cyclones are more typical as they have only one storm in each hemisphere. In addition, each of these latter twin tropical cyclogenesis events spans less than two days and 3° longitude.

The JTWC's 1997 Annual Tropical Cyclone Report (JTWC 1997) stated that each of the twin tropical cyclones considered in the present study originated within twin near-equatorial troughs associated with westerly wind bursts. In addition to these synoptic-scale westerly wind bursts, Lander and Guard (2001) observed that monthly mean equatorial westerlies stretched unusually far eastward throughout most of 1997. Persistent monsoon troughs in both hemispheres bounded these westerlies. Lander and Guard also noted that this pattern was consistent with the strong El Niño event that was occurring (Fig. 1).

The present study will further investigate the nature of the equatorial westerlies and near-equatorial troughs that preceded the twin tropical cyclogenesis events of October 1997. It will be shown that conditions were broadly favorable for tropical cyclogenesis in both hemispheres, as noted by Lander and Guard (2001) and JTWC (1997). However, a low-pass filter will show that this envelope of favorable conditions shifted eastward at 1–2 m s^{-1}. Favorable deep cyclonic vorticity and active convection appear to have been further modulated by convectively coupled ER waves, which might be related to the westerly wind bursts observed by JTWC (1997). It will be shown that a favorable combination of these two modes might be a key ingredient for these twin tropical cyclogenesis events because neither mode alone can account for all of the storms.

2. Data and methodology

a. Data

This study employs twice-daily European Centre for Medium-Range Weather Forecasting (ECMWF) gridded analyses on a 1.125° latitude–longitude grid. Previous studies have shown that gridded analyses from operational centers contain realistic structures for disturbances

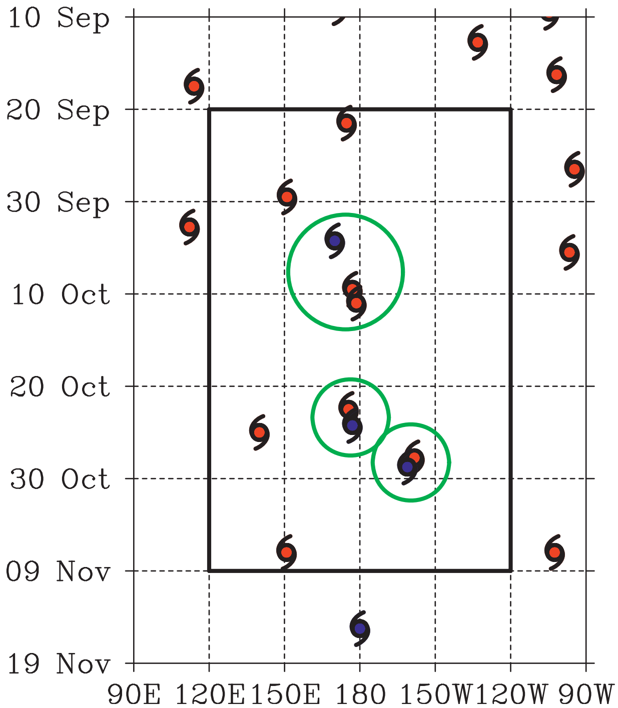

FIG. 2. Time–longitude plot of all tropical cyclogenesis events within 15° latitude of the equator. Northern Hemisphere cyclones are filled in red, Southern Hemisphere storms in blue. Green circles highlight the twin tropical cyclogenesis events. The black box indicates the region that will be focused on in Fig. 7.

in the tropics on a variety of temporal and spatial scales (e.g., Wheeler et al. 2000; Dickinson and Molinari 2002; Molinari et al. 2007). These structures were consistent with independently derived datasets such as outgoing longwave radiation (OLR).

Infrared brightness temperature (T_b) data from the Cloud Archive User Service (CLAUS; Hodges et al. 2000; Yang and Slingo 2001) of the European Union is used as a proxy for tropical convection. These data are available from the British Atmospheric Data Center (BADC; http://badc.nerc.ac.uk/data/claus/) every 3 h on a global 0.5° latitude–longitude grid. Yang et al. (2003) and others have shown that CLAUS T_b data is useful for identifying the convection coupled with equatorial waves.

The sea surface temperature (SST) associated with the twin tropical cyclones is investigated using optimum interpolation version 2 (OI.v2) monthly data obtained from NCAR. This dataset contains SST values that have been interpolated onto a 1° latitude–longitude grid by combining satellite and in situ estimates (Reynolds et al. 2002). Buoy data from the Tropical Atmosphere Ocean (TAO; McPhaden 1995) array produced virtually identical results (not shown), so the OI.v2 data is used here for its global coverage.

b. Filtering technique

The convectively coupled ER waves will be identified using a wavenumber–frequency filter that isolates westward propagation with wavenumbers 1–10 and periods 10–48 days following Frank and Roundy (2006). This filter is slightly broader than that proposed by Wheeler and Kiladis (1999), which was bounded by the ER-wave dispersion relation for equivalent depths of 8–90 m, wavenumbers less than 10, and periods less than 48 days. Roundy and Frank (2004) argued that expanding the filter beyond the shallow water dispersion curves was necessary to represent the structures observed in unfiltered data. Yang et al. (2003) similarly noted that many factors, such as background flow, surface fluxes, convection, and nonlinearities, could cause the observed waves to deviate from the linear shallow water solutions.

The low-frequency background will be examined using a simple 48-day low-pass time filter. This filter places no constraints on eastward or westward movement and simply encompasses all variations with longer periods than the ER waves. Use of a 30- or 40-day low-pass filter produced similar results (not shown), so the 48-day filter was used to prevent spectral overlap with the ER band.

An important concern when using any filter in the tropics is the potential for tropical cyclones to project onto the filter bands. It should be noted that cyclogenesis is considered here to be the first time that a storm appears in the JTWC's best-track dataset. For the present case, all of the storms have initial maximum winds of 13 m s^{-1} (25 kt) or less, with four of the seven twin tropical cyclones beginning at just 7.7 m s^{-1} (15 kt). In addition, unfiltered data show evidence of both modes several days before these cyclogenesis times. As a result, the weak tropical cyclone precursors should have a minimal impact on the filtered fields at the time of cyclogenesis.

c. Objective tracking

Determining the propagation characteristics of the apparent ER waves is fundamental to identifying them. An objective tracking technique, based on the one used by Mekonnen et al. (2006), is applied for this task. In the present study, this technique develops tracks by connecting temporal extrema of ER-band 700-hPa zonal wind $|u| > 1$ m s^{-1} and $|T_b| > 2.5$ K on a time–longitude plot. The mean phase velocities, wavelengths, and periods of these anomalies are calculated from linear best-fit lines of the tracks derived from this objective technique. All of these best-fit lines exhibit coefficients of determination (r^2) greater than 0.90. The observed ER waves appear to be convectively coupled with nearly

TABLE 1. Phase velocities (m s^{-1}) of $n = 1$ equatorial Rossby waves for various wavelengths (L) and equivalent depths (H). Values include the influence of a temporal and spatial mean background zonal flow $U = 0.7$ m s^{-1}. The effects of the zonal flow beyond simple Doppler shifting are included following Zhang and Webster (1989) and Kiladis and Wheeler (1995).

	$H =$				
L (km)	30 m	45 m	60 m	75 m	90 m
9000	−4.7	−5.7	−6.5	−7.2	−7.8
12 000	−5.0	−6.1	−7.0	−7.8	−8.5
15 000	−5.1	−6.3	−7.3	−8.1	−8.8
18 000	−5.2	−6.4	−7.4	−8.3	−9.0
21 000	−5.2	−6.5	−7.5	−8.4	−9.2

coincident zonal wind (u) and T_b anomalies. The best-fit lines derived from the u and T_b anomalies are therefore averaged together for each phase of the waves. It will be seen that the resulting phase lines generally follow the observed maxima and minima of both fields on the time–longitude plots (Fig. 7b).

The observed ER-wave phase velocities will be compared with those derived from the linear shallow water solution in the presence of a constant zonal flow U, as in Molinari et al. (2007). The value of U is estimated using the spatial and temporal mean 700-hPa zonal wind u over the series of waves (0000 UTC 20 September–0000 UTC 9 November, 10°S–10°N and 120°E–120°W), which gives $U = 0.7$ m s^{-1}. Table 1 gives the idealized ER wave phase velocities calculated for a range of equivalent depths (H) following Zhang and Webster (1989) and Kiladis and Wheeler (1995). These phase velocities include effects of the background zonal flow beyond simple Doppler shifting.

3. Results

a. Background conditions

Figure 3 presents the mean SSTs for October 1997. The hurricane symbols denote the genesis locations for each of the twin tropical cyclones. Consistent with the extreme El Niño conditions, nearly the entire equatorial Pacific exhibits SSTs in excess of 26°C. All of the twin tropical cyclones form in the central Pacific where the SST is highest on both sides of the equator.

The background atmospheric conditions are presented in Fig. 4. These plots show the 48-day low-pass-filtered data for 0000 UTC 18 October, which is the mean genesis time for the seven twin tropical cyclones. Because of the low frequency of this filter, plots created for the actual cyclogenesis dates of individual storms (not shown) are very similar except for a gradual (1–2 m s^{-1}) eastward propagation of the primary features. [The impact of this eastward propagation will be examined later in time–longitude (Fig. 7a) and time series (Fig. 8) plots.]

The low-pass-filtered T_b (shading), 1000-hPa height (contours), and 1000-hPa winds (vectors) are shown in Fig. 4a. The background convection, as indicated by depressed values of T_b, tends to be collocated with the highest SSTs (Fig. 3), except in the northwestern Pacific. That region features a broad area of warm water (SST > 29°C) but little evidence of background convection. In the eastern Pacific, the SSTs are higher in the Northern Hemisphere, and the active convection is similarly confined to the Northern Hemisphere ITCZ. The twin tropical cyclones only develop in the central Pacific where the warmest water and active background convection extend into both hemispheres.

The lowest 1000-hPa heights in Fig. 4a coincide with the ITCZ in the eastern Pacific. This trough extends westward throughout the equatorial Pacific, and all of the twin tropical cyclones form within it. The 1000-hPa winds along the equator are westerly, directed toward the height minimum. This pattern represents the persistent near-equatorial monsoon troughs that are consistent with El Niño (Lander and Guard 2001; JTWC 1997). Farther poleward, the trade easterlies converge into the convective regions. The meridional distribution of the zonal wind, with trade easterlies poleward of equatorial westerlies, produces strips of cyclonic vorticity in both hemispheres.

Figure 4b shows the low-pass-filtered 700-hPa winds and relative vorticity (shading). The trade easterlies are much weaker or, in some regions, completely absent. However, the equatorial westerlies and associated strips of cyclonic vorticity are more pronounced than at the surface (Fig. 4a). These deep low-pass features peak at 850 hPa but extend up to 400 hPa (not shown). Figure 4b is presented at 700 hPa for later comparisons with the ER-band anomalies, which peak at this level. All of the twin tropical cyclones appear to form in association with the strips of deep cyclonic vorticity. Near the ITCZ in the eastern Pacific, the cyclonic vorticity is shallower and barely reaches 700 hPa. This difference might help to account for the absence of cyclogenesis there (Fig. 2).

The low-pass-filtered scalar (shading) and vector (vectors) 850–200-hPa vertical wind shears are shown in Fig. 4c. Strong easterly shear lies along the equator while westerly shear exists farther poleward. The easterly shear along the equator arises from the lower-level equatorial westerlies feeding into the convection (Figs. 4a,b) combined with easterly outflow aloft (not shown). This pattern is similar to the Gill (1980) solution for stationary convective heating.

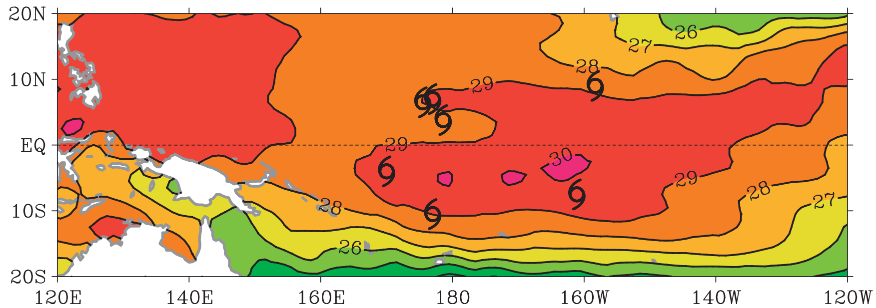

FIG. 3. Mean SST for October 1997 contoured every 1°C. Hurricane symbols denote genesis locations of the twin tropical cyclones.

Most of the twin tropical cyclones form within the strips of low vertical shear at 5°–12° latitude in both hemispheres. Two storms form closer to the equator where the scalar vertical shear is nearly 15 m s^{-1} (orange shading). However, the vector shear is easterly in this region, which some studies have shown is more favorable for cyclogenesis than westerly shear of the same magnitude (e.g., Tuleya and Kurihara 1981). The vertical wind shear is also generally small in the equatorial eastern Pacific. As noted previously, however, no twin tropical cyclones form in that region, probably because of the absence of other important ingredients (e.g., deep cyclonic vorticity, convection, and warm water in both hemispheres).

Figures 3 and 4 indicate that all of the twin tropical cyclones develop in a large and long-lasting region of favorable background conditions in both hemispheres. These favorable conditions stretch for 40° longitude, which leads to the question of why the twin tropical cyclones formed where and when they did. The synoptic evolution leading to these three twin tropical cyclogenesis events will now be examined in an attempt to answer that question.

b. Synoptic evolution

Figure 5 shows unfiltered synoptic maps at 0000 UTC every 6 days from 28 September to 28 October. Shading indicates T_b less than 270 K and the vectors represent 700-hPa winds. Hurricane symbols denote genesis locations of twin tropical cyclones within 3 days of the time plotted.

The active convection and equatorial westerlies that appeared in Figs. 4a and 4b are also prominent in Fig. 5. However, these features evolve on multiple time scales. For example, the strongest convection gradually propagates eastward during this 1-month period. On 28 September (Fig. 5a) and 4 October (Fig. 5b), the strongest convection is west of the date line, but it shifts to near 150°W by 28 October (Fig. 5f). The longitudes of the twin tropical cyclogenesis events also follow this eastward progression. The first two sets form between 170°E and the date line (Figs. 5b,c,e), whereas the final twin tropical cyclogenesis event occurs near 160°W (Fig. 5f).

In addition to the slow eastward propagation, the convection and equatorial westerlies also fluctuate on smaller scales. They strengthen (Figs. 5a–c), weaken (Fig. 5d), and then strengthen again (Figs. 5e,f). No twin tropical cyclones form near 16 October when the equatorial westerlies and convection are both weak.

To explore the evolution of these features, Fig. 6 shows time–longitude plots of unfiltered T_b averaged 10°S–10°N and 700-hPa u averaged 4.5°S–4.5°N. Tropical cyclogenesis is plotted as in Fig. 2, except now only the twin tropical cyclones are shown. The box in Fig. 6 indicates the region that will be focused on in Fig. 7 with filtered data. The gradual eastward progression of the active convection (i.e., low T_b, warm colors) is evident in Fig. 6a. The convection occurs within and slightly to the east of equatorial westerlies (Fig. 6b, warm colors), but the eastward propagation is less clear in u.

As illustrated in Fig. 5d, the convection and equatorial westerlies briefly relax near 16 October. Figure 6 suggests westward propagation of this break period in both T_b and u. The equatorial westerlies and active convection also seem to move westward at a similar velocity. Compared to the gradual eastward propagation, this westward propagating mode appears to move faster and have a much higher frequency.

c. Filtered modes

To investigate these two modes separately, Fig. 7 shows T_b (shading) and 700-hPa u (contours) that are filtered as described in the previous section. Figure 7a shows the 48-day low-pass-filtered data, while Fig. 7b presents the ER-band-filtered data. The area shown in these plots corresponds to the boxes drawn in Figs. 2 and 6.

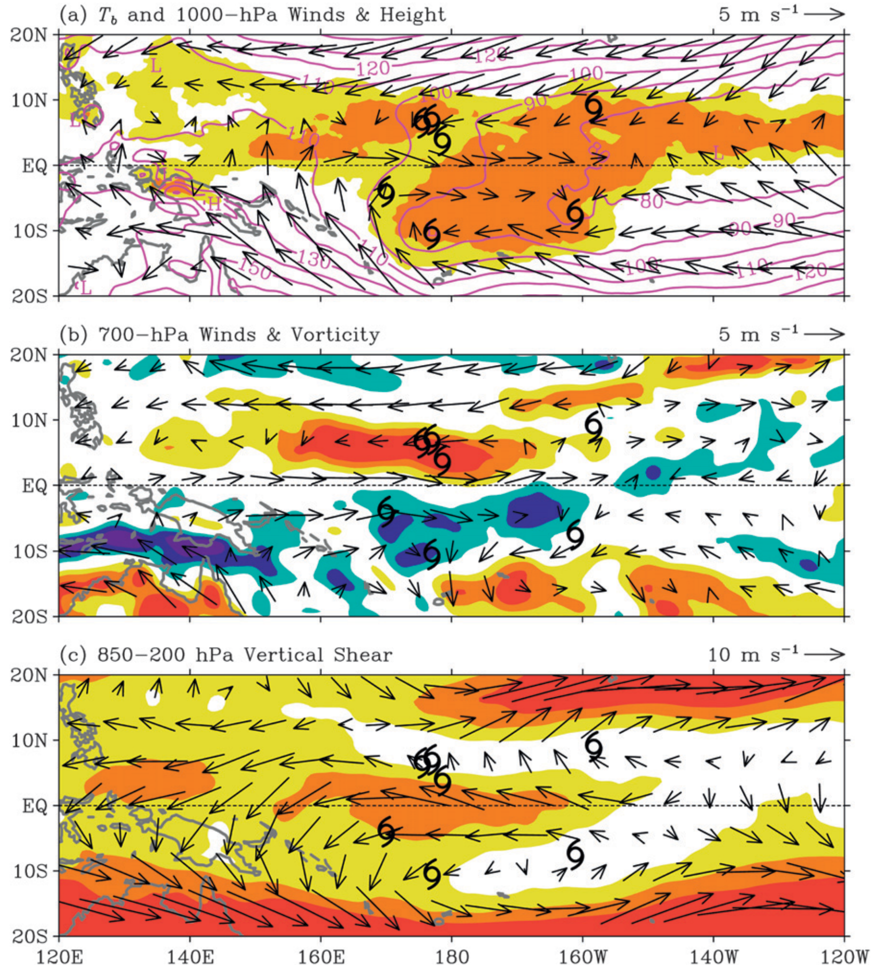

FIG. 4. Latitude–longitude plots for 0000 UTC 18 Oct 1997 of 48-day low-pass-filtered (a) T_b (shaded), 1000-hPa height (contoured) and 1000-hPa winds, (b) 700-hPa relative vorticity (shaded) and 700-hPa winds, and (c) scalar (shading) and vector (vectors) 850–200-hPa vertical wind shear. Hurricane symbols denote genesis locations of the twin tropical cyclones. (a) Shading represents T_b of 270–280 K (yellow) and <270 K (orange). (b) Relative vorticity is shaded in 5×10^{-6} s^{-1} increments with values less than -5×10^{-6} s^{-1} in cool colors and values greater than $+5 \times 10^{-6}$ s^{-1} in warm colors. (c) Scalar vertical shear greater than 10 m s^{-1} is shaded in 5 m s^{-1} intervals.

The gradual eastward propagation of the convection shows prominently in the low-pass-filtered T_b (Fig. 7a). Consistent with the unfiltered data (Fig. 6), the equatorial westerlies tend to spread eastward with the convection. The convection is concentrated in the zonally convergent region to the east of the maximum equatorial westerlies. All of the twin tropical cyclones develop in this area of convection, zonal convergence, and equatorial westerlies, which is consistent with the latitude–longitude plots in Fig. 4. The scale, structure, and eastward propagation of this convective system resemble the MJO. However, the phase velocity of the convection in Fig. 7a is only 1–2 m s^{-1}, which is slower than the 5 m s^{-1} that is typically associated with the MJO (Zhang 2005). The MJO usually has a period (40–50 days) near the cutoff of the 48-day low-pass filter used here, but other filters [e.g., a 30-day low-pass filter or the MJO-band filter from Roundy and Frank (2004)] also produced a 1–2 m s^{-1} phase velocity for the low-frequency convection (not shown). Roundy and Kiladis (2006) hypothesized that the MJO could combine with oceanic Kelvin waves to produce a coupled mode with a phase velocity similar to that observed in Fig. 7a. However, time–longitude plots of SST and ocean surface dynamic height (not shown) do not provide evidence of such a coupled mode.

The higher frequency mode seems to be captured by the ER-band filter (Fig. 7b). The twin tropical cyclones

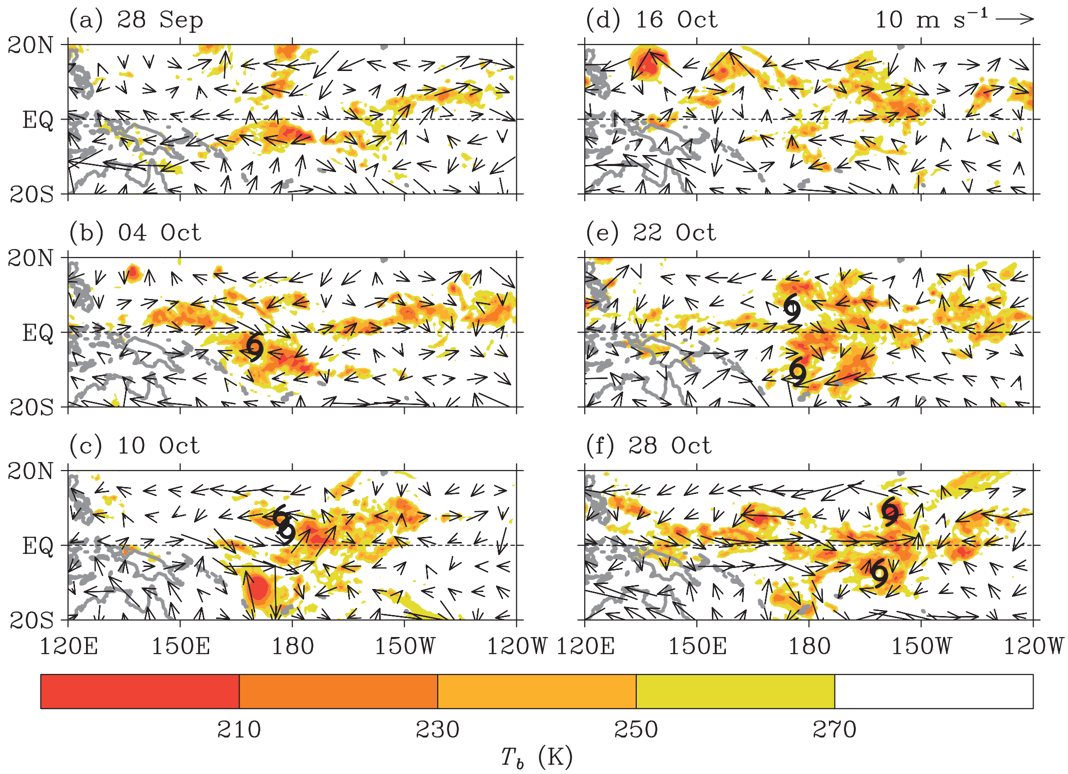

FIG. 5. Evolution of unfiltered T_b (shaded) and 700-hPa winds, shown every 6 days at 0000 UTC (a) 28 September, (b) 4 October, (c) 10 October, (d) 16 October, (e) 22 October, and (f) 28 October. Hurricanes symbols indicate genesis points of twin tropical cyclones within 3 days of the time plotted. Shading indicates $T_b < 270$ K in 20-K intervals.

tend to develop within the convective (negative T_b, shading) and equatorial westerly anomalies (red contours). Although two Northern Hemisphere storms form when this mode is nearly neutral, no twin tropical cyclones develop during the break period when the ER waves suppress convection and produce equatorial easterly anomalies. In addition, the westerly wind bursts observed by JTWC (1997) were probably associated with the westerly anomalies of the waves.

The magenta lines in Fig. 7b represent the mean best-fit phase lines for the u (contours) and T_b (shading) anomalies of each wave as described in section 2c. The mean phase velocities for the u and T_b anomalies are both -6.8 m s^{-1}, which yields some confidence in this value. However, the velocities measured from u or T_b alone range from -8.9 to -5.3 m s^{-1}. Individual measurements of the wavelength vary from 9300 to 19 800 km with a mean of 13 700 km. Similarly, measurements of the period range from 14 days to 33 days with a mean of 25 days.

In spite of these uncertainties, Table 1 shows that the observed wavelengths and phase velocities generally fit the dispersion relation for a range in equivalent depth (H) of 30–90 m. The equivalent depth for the mean wavelength (13 700 km) and mean phase velocity (-6.8 m s^{-1}) is between 45 and 60 m. All of these equivalent depths fall within the span (8–90 m) used by Wheeler and Kiladis (1999) to identify convectively coupled waves. The only other convectively coupled equatorial wave mode that can produce equatorial u anomalies with a similar period is the eastward-propagating Kelvin wave. Because the unfiltered disturbances in Fig. 6 primarily move westward, it seems reasonable to conclude that these are convectively coupled ER waves.

The shallow water solution for long ER waves, such as those described above, is nearly nondispersive (Gill 1982). The idealized phase and group velocities for these waves are both westward and within 1 m s^{-1} of each other. However, the maximum amplitudes in Fig. 7b actually move eastward, the opposite direction. The green lines in Fig. 7 represent a best-fit line following the maximum amplitudes observed in each phase of the wave. This apparent group velocity is eastward at 0.63 m s^{-1}. Figure 7a indicates that the maximum amplitudes of the waves roughly follow the western edges of the low-frequency convection and zonal convergence. Molinari et al. (2007) and references therein have shown that a zonally convergent background can amplify ER waves. In the present case, these background features gradually

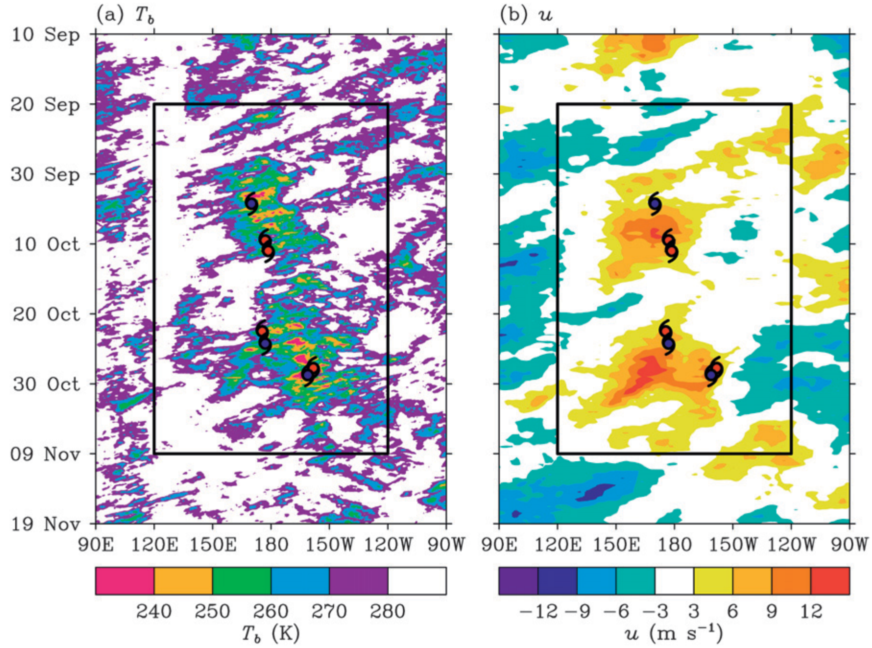

FIG. 6. Time–longitude plots of (a) unfiltered T_b averaged 10°S–10°N and (b) 700-hPa u averaged 4.5°S–4.5°N. Cyclogenesis is plotted as in Fig. 2, but now only twin tropical cyclones are shown. The black box indicates the region that will be focused on in Fig. 7.

move eastward and their effects might dominate over the weak dispersion of the waves to produce the behavior in Fig. 7.

Figure 7 suggests that neither mode alone could account for all of the twin tropical cyclones. Figure 8 shows time series plots that compare the unfiltered data (gray), low-pass-filtered data (green), ER-filtered data (red), and the sum of the two filters (black). Figures 8a,b show 700-hPa u averaged 4.5°S–4.5°N, and Figs. 8c,d show T_b averaged 10°S–10°N. The data in Figs. 8a,c are also

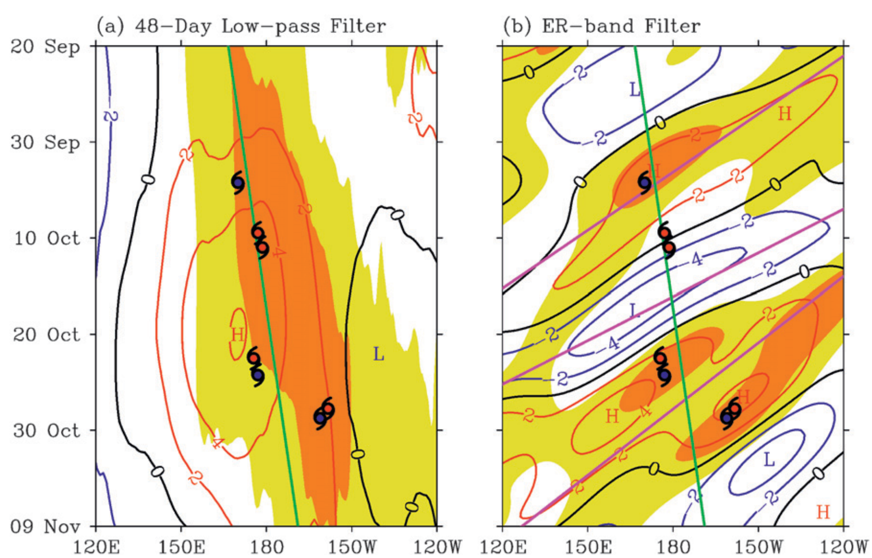

FIG. 7. Time–longitude plot of filtered T_b averaged 10°S–10°N (shaded) and 700-hPa u averaged 4.5°S–4.5°N (contoured). Twin tropical cyclones are plotted as in Fig. 6. (a) The 48-day low-pass-filtered data. Contours of u are drawn every 2 m s^{-1}, and shading represents T_b of 270–280 K (yellow) and < 270 K (orange). (b) ER-band filtered data. Contours of u are drawn as in (a), and shading indicates T_b between 0 and −5 K (yellow) and less than −5 K (orange).

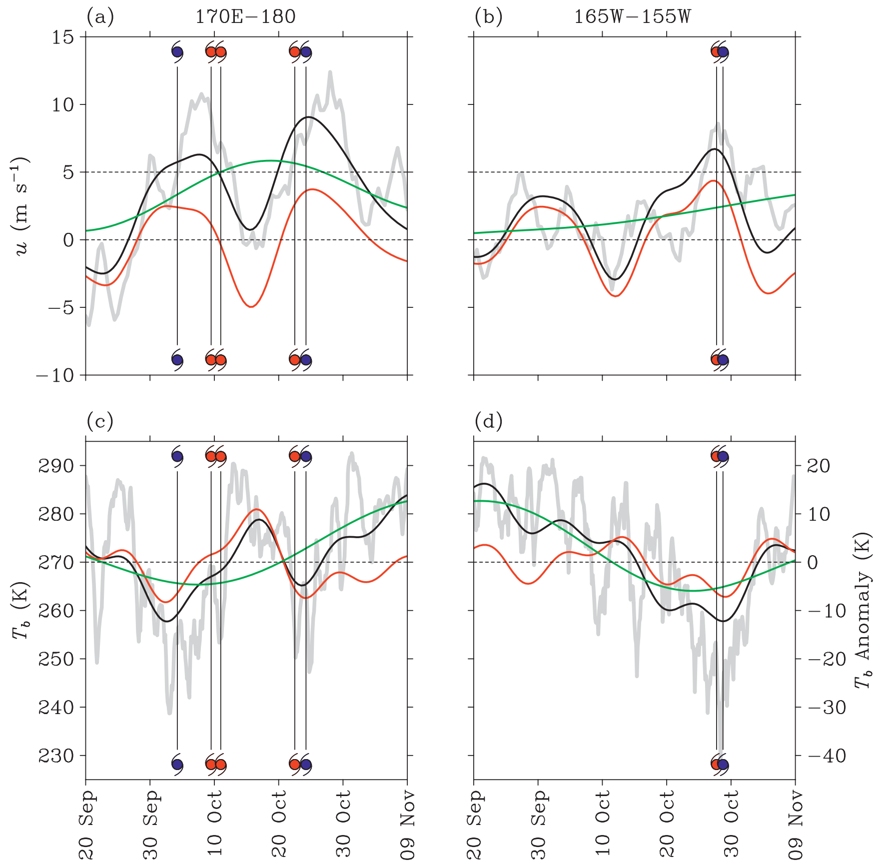

FIG. 8. Time series plots of unfiltered data (gray), low-pass filtered data (green), ER-filtered data (red), and the sum of the two filters (black). Plots show (a),(b) 700-hPa u averaged 4.5°S–4.5°N and (c),(d) T_b averaged 10°S–10°N with the ER-band data plotted with respect to the right axis. Data is also averaged longitudinally (a),(c) 170°E–180° and (b),(d) 165°–155°W. Vertical lines indicate cyclogenesis of twin tropical cyclones within the respective lon bands. Tropical cyclone symbols are drawn as in Fig. 2.

averaged longitudinally 170°E–180°, encompassing the first two sets of twin tropical cyclones. Figures 8b,d are averaged 165°–155°W, which contains the third twin tropical cyclogenesis event. The vertical lines in Fig. 8 indicate the formation of the twin tropical cyclones within their respective longitude bands.

The similarity between the black and gray lines in Fig. 8 suggests that the two filter bands qualitatively account for the broad evolution of u and T_b. Each twin tropical cyclone forms when the sum of the filters for u is greater than 5 m s^{-1} (Figs. 8a,b, black lines) and the sum for T_b is less than 270 K (Figs. 8c,d, black lines). No such relationship with cyclogenesis can be found for either mode alone. For example, two Northern Hemisphere storms form around 10 October when the low-frequency mode is favorable (Figs. 8a,c, green lines) even though the ER-band anomalies are essentially neutral (Figs. 8a,c, red lines). Conversely, the second twin tropical cyclogenesis event occurs when the low-frequency convection is weak (Fig. 8c, green line), but it is supplemented by the active ER-wave convection (Fig. 8c, red line). Therefore, both modes seem to play important roles in modulating the twin tropical cyclogenesis.

Figure 9 shows the evolution of the sum of the two filters over a 10-month period using the thresholds noted in Fig. 8. Contours are drawn for u = 5 m s^{-1} averaged 4.5°S–4.5°N. The yellow shading indicates T_b < 270 K averaged 10°S–10°N, while the orange shading shows regions in which T_b averaged 10°S–0° and 0°–10°N are both less than 270 K. Figure 9 roughly encompasses the development of the 1997–98 El Niño event and all the twin tropical cyclones associated with it using Keen's (1982) definition (green circles).

Twin tropical cyclogenesis only occurs in regions where both thresholds are satisfied. Conversely, these thresholds are rarely met simultaneously when twin tropical cyclones do not form. March 1997 presents a notable exception where both thresholds are met over a

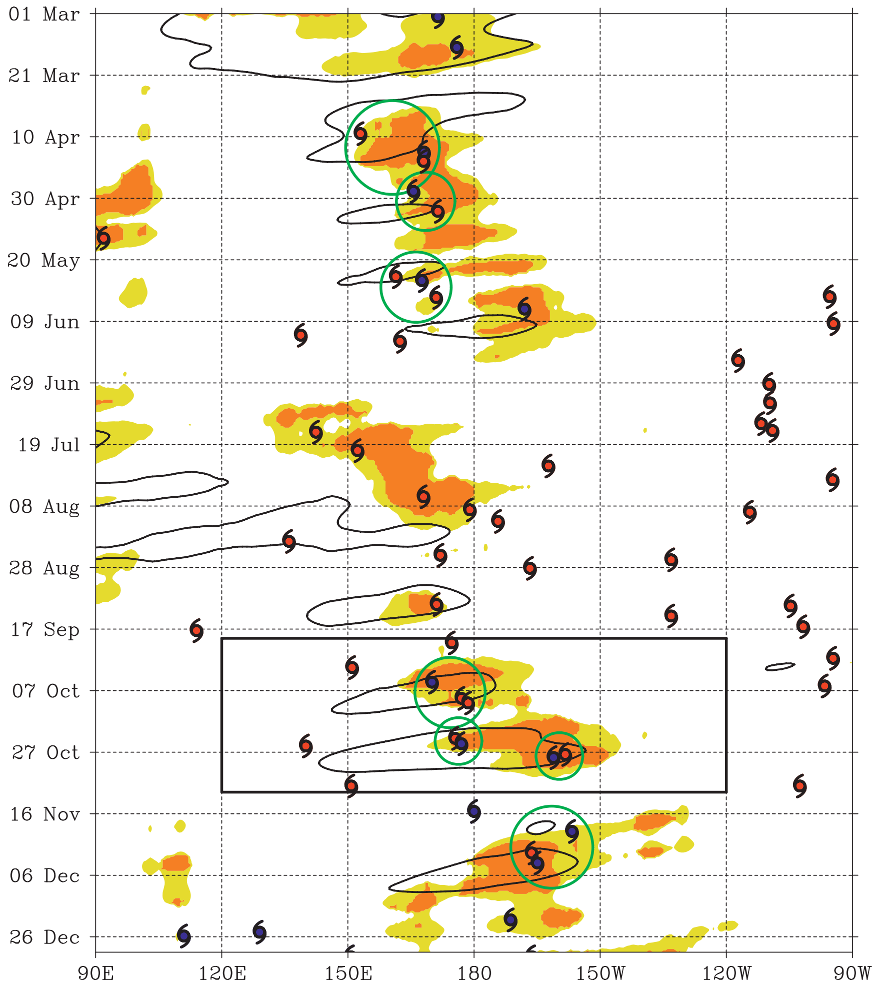

FIG. 9. Time–lon plot of the sum of the low-pass and bandpass-filtered T_b (shaded) and 700-hPa u (contoured). Tropical cyclogenesis is plotted as in Fig. 1. Green circles highlight twin tropical cyclogenesis events. The black box indicates the region that was focused on in Fig. 7. Contours show u = 5 m s^{-1} averaged 4.5°S–4.5°N. Yellow shading represents T_b < 270 K averaged 10°S–10°N, and orange shading indicates that T_b is less than 270 K when averaged *both* 10°S–0° and 0°–10°N.

broad region but only Southern Hemisphere storms form. Although Fig. 8 examined T_b averaged across the equator, Fig. 9 suggests that the enhanced convection should exist in both hemispheres to prompt twin tropical cyclogenesis. The convection is generally confined to one hemisphere during March (yellow shading), which may explain why these storms only form in the Southern Hemisphere. During each of the seven twin tropical cyclogenesis events, both hemispheres meet the 270-K threshold (orange shading).

4. Discussion

This study examined three sets of twin tropical cyclones that developed during October 1997. This outbreak represented the only one of its kind during a 37-yr period. Monthly mean SST and 48-day low-pass-filtered data showed broadly favorable conditions in both hemispheres (Figs. 3 and 4). Consistent with the strong El Niño of 1997–98, the equatorial central Pacific exhibited high SSTs and active convection. Equatorial westerlies fed into this background convection at low levels. Combined with trade easterlies farther poleward, the equatorial westerlies produced strips of cyclonic vorticity through a deep layer in both hemispheres. These strips were associated with the persistent monsoon troughs observed by Lander and Guard (2001) and JTWC (1997). The pattern was also consistent with Keen (1982), who showed that the anomalous circulation during El Niño events could foster twin tropical cyclones in the central Pacific. Each twin tropical cyclone examined here formed within these broadly favorable conditions. Time–longitude plots (Figs. 6 and 7a) indicate that this favorable envelope gradually shifted eastward.

The spatial and temporal scale of the low-frequency mode was similar to the MJO (Fig. 7a), but the observed phase velocity of 1–2 m s^{-1} was slower than the 5 m s^{-1} that is typically associated with the MJO (Zhang 2005). Roundy and Kiladis (2006) suggested that coupling with oceanic Kelvin waves could significantly reduce the phase velocity of the MJO, but plots of oceanic data (not shown) did not support a coupled mode in the present case.

In addition to providing favorable conditions for cyclogenesis, the background convection and zonal convergence associated with the low-frequency mode also appeared to intensify a series of convectively coupled ER waves (Fig. 7). These ER waves exhibited a mean phase velocity of -6.8 m s^{-1} and a mean wavelength of 13 700 km. These values fit the dispersion relation for an equivalent depth between 45 and 60 m (Table 1), which falls within the range previously observed for convectively coupled equatorial waves (e.g., Wheeler and Kiladis 1999).

Most of the twin tropical cyclones developed when the ER waves produced convective and equatorial westerly anomalies (Fig. 7b). This relationship suggests that the ER waves might have generated the westerly wind bursts observed by JTWC (1997). Consequently, the ER waves apparently favored twin tropical cyclogenesis by enhancing deep cyclonic vorticity and convection. This relationship is similar to that found by previous studies of convectively coupled equatorial waves and tropical cyclogenesis (e.g., Numaguti 1995; Dickinson and Molinari 2002; Bessafi and Wheeler 2006; Frank and Roundy 2006; Molinari et al. 2007), although none of these specifically addressed twin tropical cyclones.

Past research on twin tropical cyclogenesis focused on ER waves that were forced responses to stationary convection (e.g., Lander 1990; Ferreira et al. 1996). In the simulations by Ferreira et al., for example, the twin cyclonic vortices developed only when the heating remained stationary. However, the unfiltered T_b in the present case (Fig. 6a) seemed to be dominated by low-frequency eastward propagation and higher frequency westward movement rather than a stationary mode. The low-frequency mode (Figs. 4 and 7a) did resemble the MJO simulation by Ferreira et al. in which strips of cyclonic vorticity trailed the heating as it moved eastward. These strips probably enhanced the broad favorable conditions within which the storms formed, but the convection was never stationary and did not appear to force twin vortices as in the simulations. While the low-frequency pattern might be associated with a convectively forced ER wave, the higher frequency convection seemed to follow the idealized ER wave phase velocity. As a result, this mode was probably composed of convectively coupled ER waves rather than a forced response.

Neither the low-frequency background nor the ER waves alone could account for all of the twin tropical cyclones. The sum of the two modes in both equatorial u and T_b appeared to be more significant for cyclogenesis (Fig. 8). Each twin tropical cyclone formed when the sum of the filters produced $u > 5$ m s^{-1} and $T_b < 270$ K. Some of the twin tropical cyclones formed when one of the two modes was weak or even slightly unfavorable (Fig. 8), but in each of these cases, the other mode was favorable enough to compensate. Figure 9 supports the importance of both modes for twin tropical cyclogenesis. During the 1997–98 El Niño, twin tropical cyclones only developed in regions where both thresholds were met simultaneously.

The apparent relationship between the sum of the modes and the cyclogenesis presents an interesting forecast challenge. In real time, it is difficult to isolate modes by filtering. However, a forecast center could easily produce an unfiltered time–longitude series of equatorial zonal wind and near-equatorial convection. Figures 8 and 9 showed that increases in equatorial westerlies and convective intensity can provide a potential early warning to tropical cyclogenesis in a given latitude band. The existence of relatively long-period modes within observed fields provides an opportunity for statistical prediction of tropical cyclogenesis. Such an approach has been proposed by Frank and Roundy (2006) and Leroy and Wheeler (2008).

Twin tropical cyclones themselves might also warrant further investigation. The few climatologies that exist (Keen 1982; Lander 1990; Harrison and Giese 1991) use widely varying definitions for these events. Future research should strive to develop a systematic definition that distinguishes twin tropical cyclones from coincidental events. The interrelationship between El Niño and twin tropical cyclones addressed by Keen (1982) and Harrison and Giese (1991) might deserve renewed attention with the benefit of more satellite data and El Niño events. Contrasts should be drawn between the 1997–98 El Niño that had seven sets of twin tropical cyclones and the 1982–83 event that had none. Finally, possible feedbacks of the twin tropical cyclones onto the equatorial westerlies and El Niño should be investigated.

Acknowledgments. We extend our gratitude to Dr. Paul Roundy, Dr. Anantha Aiyyer, Dr. Ademe Mekonnen, David Vollaro, and Gareth Berry for their help and discussions during this research. The ECMWF data were obtained from the National Center for Atmospheric Research (NCAR), which is supported by the National Science Foundation. We are also grateful to Joey Comeaux of NCAR for his help with reading this data. The National Science Foundation supported this research through Grant ATM0513428.

REFERENCES

Bessafi, M., and M. C. Wheeler, 2006: Modulation of south Indian Ocean tropical cyclones by the Madden–Julian oscillation and convectively coupled equatorial waves. *Mon. Wea. Rev.,* **134,** 638–656.

Dickinson, M. J., and J. Molinari, 2002: Mixed Rossby–gravity waves and western Pacific tropical cyclogenesis. Part I: Synoptic evolution. *J. Atmos. Sci.,* **59,** 2183–2196.

Ferreira, R. N., W. N. Schubert, and J. J. Hack, 1996: Dynamical aspects of twin tropical cyclones associated with the Madden–Julian oscillation. *J. Atmos. Sci.,* **53,** 929–945.

Frank, W. M., and P. E. Roundy, 2006: The role of tropical waves in tropical cyclogenesis. *Mon. Wea. Rev.,* **134,** 2397–2417.

Gill, A. E., 1980: Some simple solutions for heat-induced tropical circulation. *Quart. J. Roy. Meteor. Soc.,* **106,** 447–462.

——, 1982: *Atmosphere–Ocean Dynamics*. Academic Press, 662 pp.

Harrison, D. E., and B. S. Giese, 1991: Episodes of surface westerly winds as observed from islands in the western tropical Pacific. *J. Geophys. Res.,* **96,** 3221–3237.

Hodges, K. I., D. W. Chappell, G. J. Robinson, and G. Yang, 2000: An improved algorithm for generating global window brightness temperatures from multiple satellite infrared imagery. *J. Atmos. Oceanic Technol.,* **17,** 1296–1312.

JTWC, 1997: 1997 annual tropical cyclone report. Joint Typhoon Warning Center.

Keen, R. A., 1982: The role of cross-equatorial tropical cyclone pairs in the southern oscillation. *Mon. Wea. Rev.,* **110,** 1405–1416.

Kiladis, G. N., and M. Wheeler, 1995: Horizontal and vertical structure of observed tropospheric equatorial Rossby waves. *J. Geophys. Res.,* **100,** 1924–1938.

Lander, M. A., 1990: Evolution of the cloud pattern during the formation of tropical cyclone twins symmetrical with respect to the equator. *Mon. Wea. Rev.,* **118,** 1194–1202.

——, and C. P. Guard, 2001: Western North Pacific, north Indian Ocean, and Southern Hemisphere tropical cyclones of 1997. *Mon. Wea. Rev.,* **129,** 3015–3036.

Leroy, A., and M. C. Wheeler, 2008: Statistical prediction of weekly tropical cyclone activity in the Southern Hemisphere. *Mon. Wea. Rev.,* **136,** 3637–3654.

Liebmann, B., H. H. Hendon, and J. D. Glick, 1994: The relationship between tropical cyclones of the western Pacific and Indian Oceans and the Madden–Julian oscillation. *J. Meteor. Soc. Japan,* **72,** 401–411.

Madden, R. A., and P. R. Julian, 1971: Detection of a 40–50 day oscillation in the zonal wind in the tropical Pacific. *J. Atmos. Sci.,* **28,** 702–708.

Matsuno, T., 1966: Quasi-geostrophic motions in the equatorial area. *J. Meteor. Soc. Japan,* **44,** 25–43.

McPhaden, M. J., 1995: The Tropical Atmosphere Ocean array is completed. *Bull. Amer. Meteor. Soc.,* **76,** 739–741.

Mekonnen, A., C. D. Thorncroft, and A. R. Aiyyer, 2006: Analysis of convection and its association with African easterly waves. *J. Climate,* **19,** 5405–5421.

Molinari, J., K. Lombardo, and D. Vollaro, 2007: Tropical cyclogenesis within an equatorial Rossby wave packet. *J. Atmos. Sci.,* **64,** 1301–1317.

Numaguti, A., 1995: Characteristics of 4-to-20-day-period disturbances observed in the equatorial Pacific during the TOGA COARE IOP. *J. Meteor. Soc. Japan,* **73,** 353–377.

Reynolds, R. W., N. A. Rayner, T. M. Smith, D. C. Stokes, and W. Wang, 2002: An improved in situ and satellite SST analysis for climate. *J. Climate,* **15,** 1609–1625.

Roundy, P. E., and W. M. Frank, 2004: A climatology of waves in the equatorial region. *J. Atmos. Sci.,* **61,** 2105–2132.

——, and G. N. Kiladis, 2006: Observed relationships between oceanic Kelvin waves and atmospheric forcing. *J. Climate,* **19,** 5253–5272.

Takayabu, Y. N., 1994: Large-scale cloud disturbances associated with equatorial waves. Part I: Spectral features of the cloud disturbances. *J. Meteor. Soc. Japan,* **72,** 433–448.

Tuleya, R. E., and Y. Kurihara, 1981: A numerical study of the effects of environmental flow on tropical storm genesis. *Mon. Wea. Rev.,* **109,** 2487–2506.

Wheeler, M., and G. N. Kiladis, 1999: Convectively coupled equatorial waves: Analysis of cloud and temperature in the wavenumber–frequency domain. *J. Atmos. Sci.,* **56,** 374–399.

——, ——, and P. J. Webster, 2000: Large-scale dynamical fields associated with convectively coupled equatorial waves. *J. Atmos. Sci.,* **57,** 613–640.

Yang, G.-Y., and J. Slingo, 2001: The diurnal cycle in the tropics. *Mon. Wea. Rev.,* **129,** 784–801.

——, B. Hoskins, and J. Slingo, 2003: Convectively coupled equatorial waves: A new methodology for identifying wave structures in observational data. *J. Atmos. Sci.,* **60,** 1637–1654.

Zhang, C., 2005: Madden–Julian oscillation. *Rev. Geophys.,* **43,** RG2003, doi:10.1029/2004RG000158.

——, and P. J. Webster, 1989: Effects of zonal flows on equatorially trapped waves. *J. Atmos. Sci.,* **46,** 3632–3652.